

# Long-Term Behavior of the Atlantic Interhemispheric SST Gradient in the CMIP5 Historical Simulations

JOHN C. H. CHIANG AND C.-Y. CHANG\*

*Department of Geography, and Berkeley Atmospheric Sciences Center, University of California, Berkeley, Berkeley, California*

M. F. WEHNER

*Lawrence Berkeley National Laboratory, Berkeley, California*

(Manuscript received 19 July 2012, in final form 17 May 2013)

## ABSTRACT

Multidecadal and longer changes to the Atlantic interhemispheric sea surface temperature gradient (AITG) in phase 5 of the Coupled Model Intercomparison Project (CMIP5) historical simulations are investigated. Observations show a secular trend to this gradient over most of the twentieth century, with the southern lobe warming faster relative to its northern counterpart. A previous study of phase 3 of the CMIP (CMIP3) suggests that this trend is partially forced by anthropogenic sulfate aerosols. This analysis collectively confirms the partially forced trend for the CMIP5 and by anthropogenic aerosols. Like the CMIP3, the CMIP5 also simulates a reversal in the AITG trend in the late 1970s, which was attributed to a leveling off of the anthropogenic aerosol influence and increased influence of greenhouse gases in the late twentieth century. Two (of 25) CMIP5 models, however, systematically simulate a twentieth-century trend opposite to observed, leading to some uncertainty regarding the forced nature of the AITG trend. The observed AITG also exhibits a pronounced multidecadal modulation on top of the trend, associated with the Atlantic multidecadal oscillation (AMO). Motivated by a recent suggestion that the AMO is a forced response to aerosols, the causes of this multidecadal behavior were also examined. A few of the CMIP5 models analyzed do produce multidecadal AITG variations that are correlated to the observed AMO-like variation, but only one, the Hadley Centre Global Environmental Model, version 2 (HadGEM2), systematically simulates AMO-like behavior with both the requisite amplitude and phase. The CMIP5 simulations thus point to a robust aerosol influence on the historical AITG trend but not to the AMO-like multidecadal behavior.

## 1. Introduction

The Atlantic interhemispheric sea surface temperature gradient (AITG) exerts strong control on rainfall in the tropical Atlantic sector (Cox et al. 2008; Hastenrath and Heller 1977; Moura and Shukla 1981). There is an observed trend to this gradient over the twentieth century (Fig. 1), implying that the tropical Atlantic intertropical convergence zone shifted southward with the AITG given the tight coupling between the ITCZ position and cross-equatorial sea surface temperature

(SST) gradient (e.g., Chang et al. 2000; Chiang et al. 2002). Chang et al. (2011) were the first to show this long-term southward ITCZ displacement and analyze its causes, with phase 3 of the Coupled Model Intercomparison Project (CMIP3; Meehl et al. 2007) simulations showing that anthropogenic sulfate aerosols forced at least a part of the twentieth-century trend. They also identified a reversal to this trend around 1980, possibly related to regulations limiting atmospheric pollution in Europe and North America in the 1970s.

The prevailing view of this hemispheric asymmetry in the long-term tropical Atlantic SST evolution is because of the cooling effect of anthropogenic (primarily sulfate) aerosols, located and acting mostly in the Northern Hemisphere. The role of anthropogenic aerosols in further shifting the tropical rainbands southward was originally suggested in studies with atmospheric general circulation models coupled to thermodynamic “slab” ocean

---

\* Current affiliation: Risk Management Solutions, Fremont, California.

---

Corresponding author address: John C. H. Chiang, 547 McCone Hall, University of California, Berkeley, Berkeley, CA 94720-4740.  
E-mail: jch\_chiang@berkeley.edu

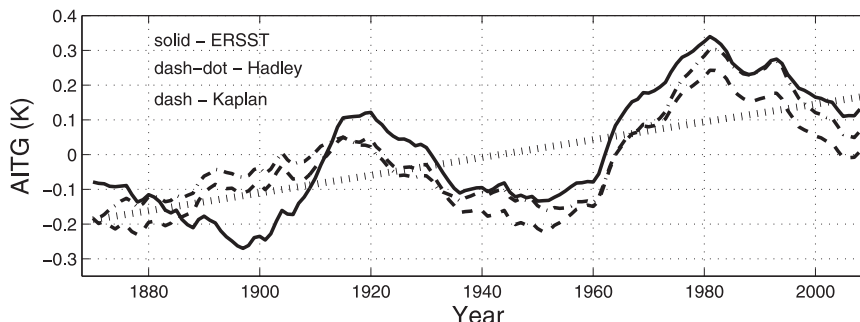


FIG. 1. The observed AITG index, defined as the SST difference between the north ( $5^{\circ}$ – $35^{\circ}$ N,  $0^{\circ}$ – $80^{\circ}$ W) and south ( $5^{\circ}$ – $35^{\circ}$ S,  $60^{\circ}$ W– $20^{\circ}$ E) tropical Atlantic, south minus north. Each line is from an observational SST dataset as denoted: Extended Reconstructed SST, version 3b (ERSST.v3b; Smith et al. 2008); Hadley Centre Sea Ice and Sea Surface Temperature dataset (HadSST; Rayner et al. 2003); and Kaplan extended SST, version 2 (Kaplan et al. 1998). The dotted straight line is the linear least squares best-fit line to the average of the three curves.

models (Rotstayn and Lohmann 2002; Williams et al. 2001). An atmospheric teleconnection is thought to connect the largely extratropical thermal forcing by the aerosols to the tropical climate, specifically altering the Hadley circulation, and recent studies have begun to elucidate its mechanisms [see the review paper by Chiang and Friedman (2012)]. Another possibility is a weakening Atlantic meridional overturning circulation (AMOC) induced by the twentieth-century climate forcing, which would have a similar effect on the AITG.

Historical simulations (Taylor et al. 2012) from phase 5 of the CMIP (CMIP5) present an opportunity to test the conclusions of Chang et al. (2011). While the CMIP5-class models evolved from the CMIP3-class models and so the test cannot be construed as independent, recent advances in representing the radiative effects of aerosols in the CMIP5-class models, including the now near-universal inclusion of indirect effects, makes this analysis meaningful and worthwhile. Furthermore, the extratropical thermal influence to the tropical rainband is thought to be sensitive to the strength of cloud radiative feedbacks (Kang et al. 2009); cloud feedbacks were also a target for extensive CMIP5-class model improvements.

This study extends the original investigation by Chang et al. (2011) by examining multidecadal variations in the AITG, which are quite pronounced (Fig. 1) and shown by Chang et al. (2011) to be tied to the Atlantic multidecadal oscillation (AMO), a prominent multidecadal variation to the basinwide North Atlantic SST. It had previously been assumed that the AMO was internal to the climate system (e.g., Ting et al. 2009), but a recent study by Booth et al. (2012) has suggested that the AMO was, in fact, largely a forced response to anthropogenic and volcanic aerosols. Given that sulfate aerosols force the AITG trend, the Booth et al. (2012) result suggests

that the multidecadal modulation of the AITG could similarly be forced. Related to this, Chang et al. (2011) also found a reversal to the forced AITG trend after 1980, which they speculated was due to the reduction in  $\text{SO}_2$  emissions with the advent of air pollution controls.

Our revisit of the long-term AITG behavior examines two issues: (i) does the CMIP5 support the Chang et al. (2011) conclusions and (ii) are there forced multidecadal variations in the AITG that are consistently expressed across the CMIP5 multimodel ensemble, specifically an AMO-like response?

## 2. Data

Table 1 details the CMIP5 models/simulations included this analysis, from the Earth System Grid (<http://pcmdi3.llnl.gov/esgcat/home.htm>). There are 85 historical ensemble members across 24 different models spanning 1850–2005; these simulations are forced with the entire suite of time-varying anthropogenic and natural forcings. The models used constitute a sizable fraction of what is available in the CMIP5 archive (17 of 26 modeling groups are represented). The bulk of the members used in our analysis (models 1–18: 71 members) were included in our initial analysis in late 2011, taken from what was then available (simulations were still being archived at that time). Models 19–24 (14 members) were added in the revision stage, to increase the representation of modeling groups in the analysis. As such, the choice of models from the CMIP5 pool was essentially random (based on their availability at time of initial analysis), and they also constitute a sizable fraction of the pool. We are, thus, confident that the output used in our analysis is representative of the population of CMIP5 historical simulations. For comparison to the forced historical simulations, we use the last 239 yr of the

TABLE 1. List of CMIP5 models used in this study. The descriptions of the first six columns are as follows, from left to right: model number; numerical identifier (ID) for ensemble members (used in reference to the EOF loadings); abbreviated name of model; expanded name of each model; aerosol indirect effect (AIE), where model is marked as “Y” if indirect effects are parameterized in model and “N” otherwise; and number of historical runs for that particular model and how many use TS or TAS. The final eight columns indicate the number of single-forcing runs for each particular model used in our analysis (blank entry indicates no runs available): all anthropogenic (Ant), anthropogenic aerosols (AA), greenhouse gases (GHG), land-use change (LU), all natural (Nat), ozone (Oz), tropospheric and stratospheric, solar (Sl), and volcanic (Vi).

| No.                  | ID    | Name           | Expansion   | AIE | Historical<br>(TS/TAS) | Ant | AA | GHG | LU | Nat | Oz | Sl | Vi |    |    |    |    |    |   |
|----------------------|-------|----------------|---|-----|------------------------|-----|----|-----|----|-----|----|----|----|----|----|----|----|----|---|
| 1                    | 1–6   | CCSM4          | Community Climate System Model, version 4   | N   | 6 (4 TS, 2 TAS)        | 4   | 3  | 1   | 2  | 1   | 2  | 1  | 3  |    |    |    |    |    |   |
| 2                    | 7–16  | CNRM-CM5       | Centre National de Recherches Météorologiques Coupled Global Climate Model, version 5   | Y   | 10 (1 TS, 9 TAS)       | 10  | —  | 6   | —  | 6   | —  | —  | —  |    |    |    |    |    |   |
| 3                    | 17–26 | CSIRO Mk3.6.0  | Commonwealth Scientific and Industrial Research Organisation Mark, version 3.6.0  | Y   | 10 (TAS)               | 5   | 5  | —   | —  | 5   | —  | —  | 5  |    |    |    |    |    |   |
| 4                    | 27–31 | CanESM2        | Second Generation Canadian Earth System Model   | Y   | 5 (TS)                 | —   | 5  | 5   | 5  | 5   | —  | 5  | —  |    |    |    |    |    |   |
| 5                    | 32–36 | GISS-E2H       | Goddard Institute for Space Studies Model E, coupled with the HYCOM ocean model   | Y   | 5 (TS)                 | 5   | 5  | —   | —  | 5   | —  | 5  | —  |    |    |    |    |    |   |
| 6                    | 37–41 | GISS-E2-R      | Goddard Institute for Space Studies Model E, coupled with the Russell ocean model   | Y   | 5 (TS)                 | 10  | 5  | 3   | 5  | 5   | 5  | 5  | —  |    |    |    |    |    |   |
| 7                    | 42–45 | HadCM3         | Hadley Centre Coupled Model, version 3  | Y   | 4 (TS)                 | —   | —  | —   | —  | —   | —  | —  | —  |    |    |    |    |    |   |
| 8                    | 46    | HadGEM2-CC     | Hadley Centre Global Environment Model, version 2—Carbon Cycle  | Y   | 1 (TS)                 | —   | —  | —   | —  | —   | —  | —  | —  |    |    |    |    |    |   |
| 9                    | 47–50 | HadGEM2-ES     | Hadley Centre Global Environment Model, version 2 (Earth System)  | Y   | 4 (TS)                 | —   | —  | 4   | —  | 3   | —  | —  | —  |    |    |    |    |    |   |
| 10                   | 51    | IPSL-CM5A-LR   | L’Institut Pierre-Simon Laplace Coupled Model, version 5, coupled with Nucleus for European Modelling of the Ocean (NEMO), low resolution | Y   | 1 (TS)                 | 3   | 1  | 1   | —  | 3   | —  | —  | —  |    |    |    |    |    |   |
| 11                   | 52    | MIROC5         | Model for Interdisciplinary Research on Climate, version 5  | Y   | 1 (TS)                 | —   | —  | —   | —  | —   | —  | —  | —  |    |    |    |    |    |   |
| 12                   | 53    | MIROC-ESM-CHEM | Model for Interdisciplinary Research on Climate, Earth System Model, Chemistry Coupled  | Y   | 1 (TS)                 | —   | —  | —   | —  | 1   | —  | —  | —  |    |    |    |    |    |   |
| 13                   | 54–56 | MIROC-ESM      | Model for Interdisciplinary Research on Climate, Earth System Model   | Y   | 3 (TS)                 | —   | —  | —   | —  | 3   | —  | —  | —  |    |    |    |    |    |   |
| 14                   | 57–59 | MPI-ESM-LR     | Max Planck Institute Earth System Model, low resolution   | Y   | 3 (TS)                 | —   | —  | —   | —  | —   | —  | —  | —  |    |    |    |    |    |   |
| 15                   | 60–64 | MRI-CGCM3      | Meteorological Research Institute Coupled Atmosphere–Ocean General Circulation Model, version 3   | Y   | 5 (TS)                 | —   | —  | —   | —  | 1   | —  | —  | —  |    |    |    |    |    |   |
| 16                   | 65–67 | NorESM1-M      | Norwegian Earth System Model, version 1 (intermediate resolution)   | Y   | 3 (2 TS, 1 TAS)        | —   | 1  | 1   | —  | 1   | —  | —  | —  |    |    |    |    |    |   |
| 17                   | 68–70 | BCC-CSM1.1     | Beijing Climate Center, Climate System Model, version 1.1   | N   | 3 (TS)                 | —   | —  | —   | —  | 1   | —  | —  | —  |    |    |    |    |    |   |
| 18                   | 71    | INM-CM4.0      | Institute of Numerical Mathematics Coupled Model, version 4.0   | N   | 1 (TS)                 | —   | —  | —   | —  | —   | —  | —  | —  |    |    |    |    |    |   |
| 19                   | 72    | ACCESS1.0      | Australian Community Climate and Earth-System Simulator, version 1.0  | Y   | 1 (TS)                 | —   | —  | —   | —  | —   | —  | —  | —  |    |    |    |    |    |   |
| 20                   | 73    | ACCESS1.3      | Australian Community Climate and Earth-System Simulator, version 1.3  | Y   | 1 (TS)                 | —   | —  | —   | —  | —   | —  | —  | —  |    |    |    |    |    |   |
| 21                   | 74–76 | CESM1 (CAM5)   | Community Earth System Model, version 1 (Community Atmosphere Model, version 5)   | Y   | 3 (TS)                 | —   | —  | —   | —  | —   | —  | —  | —  |    |    |    |    |    |   |
| 22                   | 77–81 | GFDL CM3       | Geophysical Fluid Dynamics Laboratory Climate Model, version 3  | Y   | 5 (TS)                 | 3   | 3  | —   | —  | 3   | —  | —  | —  |    |    |    |    |    |   |
| 23                   | 82–84 | GFDL-ESM2G     | Geophysical Fluid Dynamics Laboratory Earth System Model with Generalized Ocean Layer Dynamics (GOLD) component                           | Y   | 3 (TS)                 | —   | —  | —   | —  | —   | —  | —  | —  |    |    |    |    |    |   |
| 24                   | 85    | GFDL-ESM2M     | Geophysical Fluid Dynamics Laboratory Earth System Model with Modular Ocean Model 4 (MOM4) component                                      | Y   | 1 (TS)                 | 1   | 1  | 1   | 1  | 1   | 1  | 1  | 1  |    |    |    |    |    |   |
| Total number of runs |       |                |   |     |                        |     |    |     |    |     | 85 | 41 | 29 | 22 | 13 | 44 | 12 | 14 | 9 |

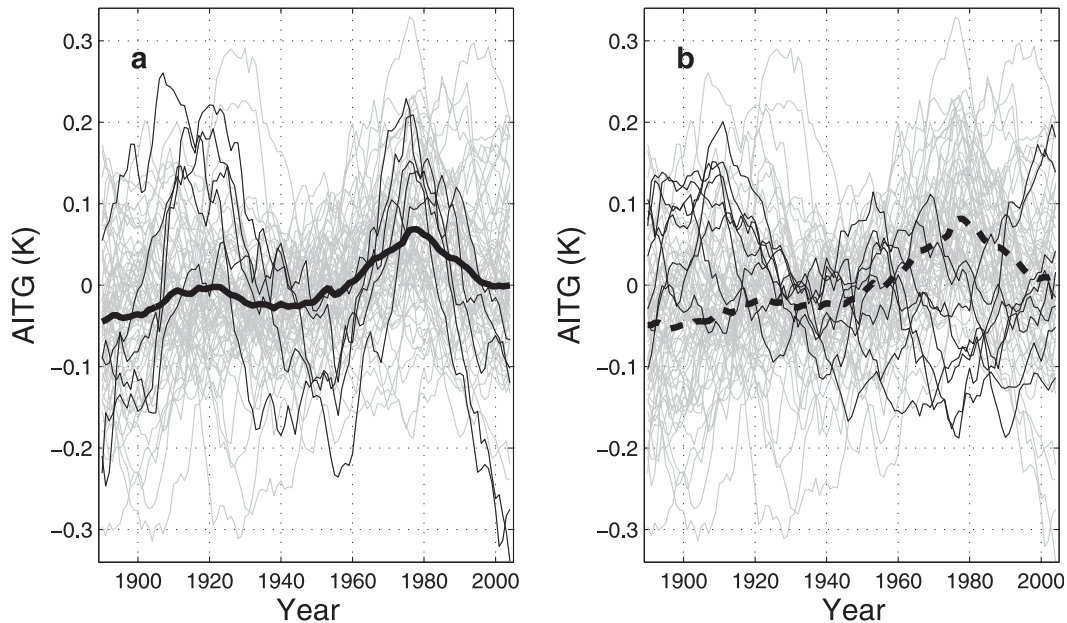


FIG. 2. AITG indices in the CMIP5 historical simulations. (a) AITG indices simulated by each ensemble member (light gray lines) and the multimodel ensemble mean (thick black line). As a whole, the simulated AITG exhibit a progressive upward trend over the twentieth century but with significant variation between individual ensemble members. The five HadGEM2 AITG simulations are highlighted as thin black lines, showing the pronounced AMO-like multidecadal variation. (b) Light gray lines are the AITG indices simulated by each ensemble member, as in (a). The thin black lines show the MPI-ESM-LR and MRI-CGCM3 AITG simulations, each exhibiting a downward trend that is at variance with the AITG simulations by the other models. The thick dashed line is the multimodel ensemble mean excluding the HadGEM, MPI, and MRI models.

corresponding preindustrial simulations where climate forcings are kept constant in time. We also examine a number of single-forcing simulations (Table 1) spanning the historical period but with only one (or a subset) of the time-varying forcings applied.

Following Chang et al. (2011), we defined an AITG index by subtracting the average SST across the entire tropical–subtropical North Atlantic basin ( $5^{\circ}$ – $35^{\circ}$ N,  $0^{\circ}$ – $80^{\circ}$ W) from the tropical–subtropical South Atlantic ( $5^{\circ}$ – $35^{\circ}$ S,  $60^{\circ}$ W– $20^{\circ}$ E), south minus north. Monthly anomalies are calculated by removing the long-term climatology (taken over the 1890–2004 period), and a 21-yr running mean is subsequently applied to the monthly anomaly in order to emphasize multidecadal and longer-term variations. The mean for each year is then calculated, and all subsequent analyses use this annual-resolution time series. The same procedure is used for both the observed and simulated AITG indices.

In a few instances (see Table 1), we used the surface air temperature (TAS) variable when the surface temperature (TS) variable was not available; this was done to maximize the number of models included in the analysis. We found the AITG indices thus constructed be virtually identical when both variables were available for a particular ensemble member. This is not surprising

given the close correspondence between SST and surface air temperature on longer time scales.

As a first cut, we visually examine the CMIP5 AITG time series as a “spaghetti” diagram with all member time series overlaid (Fig. 2a). There is significant variation between ensemble member simulations of the AITG, but there is a discernible upward trend within the spaghetti that is confirmed in the multimodel mean (Fig. 2a, thick black line). There is also an apparent multidecadal modulation in the mean, with peaks around 1920 and 1980. We point out features apparent in this visual analysis that will be discussed in depth later on:

- 1) The HadGEM2 simulations (Fig. 2a, thin black lines) exhibit a pronounced multidecadal variation comparable in phase and amplitude to the influence by the AMO on the AITG.
- 2) Two models (MPI-ESM-LR and MRI-CGCM3) systematically simulate a decreasing trend over the historical period, at variance with the other model simulations (Fig. 2b, thin black lines).
- 3) If these model “outliers” (HadGEM2, MPI-ESM-LR, and MRI-CGCM3) are not included in the multimodel ensemble mean, the resulting mean AITG (Fig. 2b, thick dashed line) exhibits less of the peak

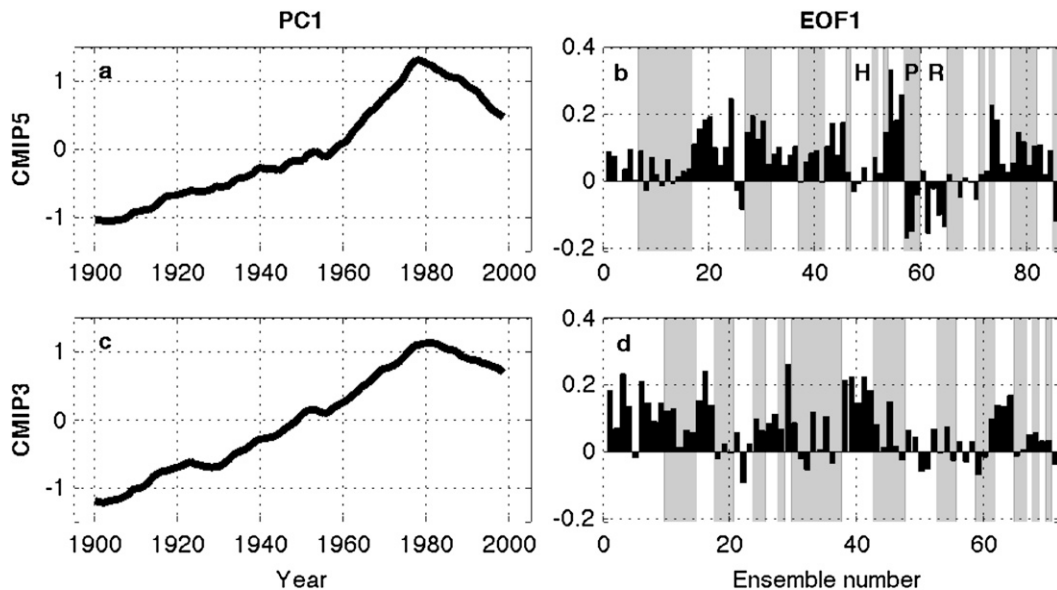


FIG. 3. Results of EOF analyses on the AITG indices. (a) PC1 and (b) corresponding EOF of the 85-member AITG indices from CMIP5. EOF1 explains 44% of the total variance. The order of the models in the EOF loadings is as indicated in Table 1, and gray/white shading on the EOF demarcates the loadings for the same model. The “H” indicates the location of the loadings for the HadGEM2-ES ensemble members (the lone HadGEM2-CC is the entry immediately to its left), “P” is for the MPI-ESM-LR ensemble members, and “R” is for the MRI-CGCM3. The EOF exhibits an upward trend, and most models project positively on EOF1, indicating that this upward trend in the AITG occurs in most twentieth-century model simulations. Because the EOF analysis was applied on normalized AITG indices, the EOFs and projection coefficients are dimensionless. (c),(d) As in (a),(b), but for the CMIP3 models (Chang et al. 2011). Here, EOF1 explains 47% of the total variance. The order of the CMIP3 EOF loadings is as presented in Fig. 3 of Chang et al. (2011).

around 1920. However, the peak around 1980 is still prominent, as is the turnaround in the AITG trend. The ensemble-mean AITG thus appears to have two periods of upward trends: a smaller one from the late 1800s to ~1920 and a more pronounced upward trend from the mid-1940s to the late 1970s.

### 3. EOF and trend analysis

In this section, we repeat the Chang et al. (2011) analysis on the AITG historical simulations, but with the CMIP5 multimodel ensemble, and discuss similarities and differences between the two results.

#### a. CMIP5 historical results

Following Chang et al. (2011), we extract the “most common” AITG behavior in the historical simulations from 1900 to 1998 by applying an empirical orthogonal function (EOF; Barnett 1977) analysis collectively on the 71 model AITG indices. The “stations” that usually refer to spatial grid points in conventional EOF applications on climate data here represent individual ensemble members. Prior to analysis, each index was normalized by the standard deviation of the AITG index from the corresponding

model’s preindustrial simulation. As such, we weight each ensemble member equally, thus treating each member as a possible realization of the climate. The other choice was to weight by model, but in the absence of a compelling reason we decided rather to weight each ensemble member equally as it makes the least assumptions regarding the properties of the model simulations.

The first principal component (PC1; Fig. 3a), accounting for 44% of the total variance, shows a trend for most of the twentieth century with a turnaround in the late 1970s. The EOF1 loadings (Fig. 3b) are predominantly positive, indicating that most (though not all; see section 3c) of the ensemble members simulate this trend behavior and in the same sense. In this regard, the CMIP5 EOF1 results are quite similar to the CMIP3 results in the variance explained (44% for the CMIP5 versus 47% for the CMIP3), the structure of PC1, and also in that the EOF1 loadings are mostly of the same sign (cf. Figs. 3a,b for the CMIP5 and Figs. 3c,d for the CMIP3). As a check, the multimodel ensemble-mean AITG (in particular Fig. 2b shows the mean taken over all models excluding the outlier HadGEM2, MPI-ESM-LR, and MRI-CGCM3) closely resemble PC1, including the late 1970s turnaround.

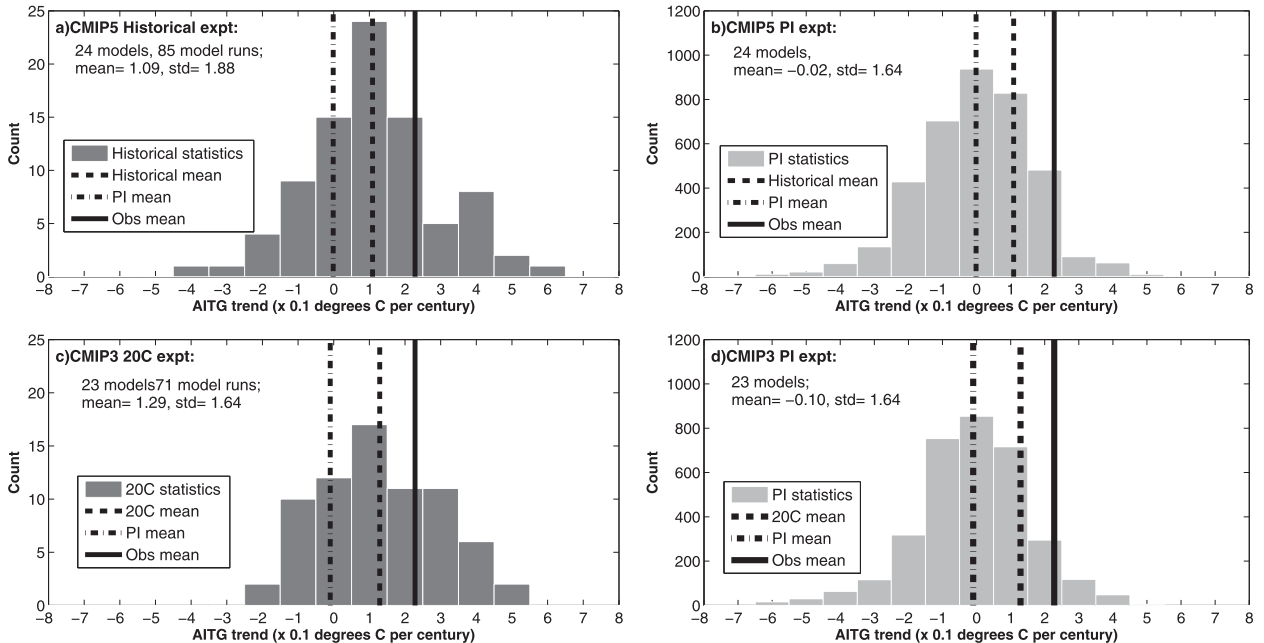


FIG. 4. Statistics of 83-yr trends of the modeled AITG indices from the CMIP5 (a) historical and (b) preindustrial simulations. The distribution of slopes of the trends computed from each of the 85 historical simulations; the y axis counts the number of members in each bin with the trend magnitudes as shown on the x axis. Also shown is the ensemble-mean slope magnitude (dashed line), mean of the preindustrial slope distribution (dashed–dotted line), and the observed slope magnitude (solid line). The observed slope value is the average trend of the three observed AITG estimates shown in Fig. 1a: the Kaplan SST dataset ( $0.158^{\circ}\text{C century}^{-1}$ ), HadISST ( $0.188^{\circ}\text{C century}^{-1}$ ), and ERSST.v3b ( $0.358^{\circ}\text{C century}^{-1}$ ). (b) The distribution of slopes computed from the corresponding preindustrial simulations; the lines are drawn as in (a). The y axis counts the number of evaluated 83-yr intervals in the preindustrial simulations with the trend magnitudes shown on the x axis. (c),(d) As in (a),(b), but for the CMIP3 (Chang et al. 2011).

We note in passing that the HadGEM2 simulations essentially do not project onto mode 1 (Fig. 3b) and hence do not contribute to the inferred CMIP5 multimodel AITG trend behavior. Moreover, the turnaround in the AITG trend after the late 1970s is not dependent on the HadGEM2 contribution: this is clearly apparent in Fig. 1b, where the multimodel mean excluding HadGEM2, MPI-ESM-LR, and MRI-CGCM3 still exhibits the turnaround in the AITG trend.

Following Chang et al. (2011), we calculate the slope of the AITG trend from 1900 to 1982 for each ensemble member to form a distribution of slopes (Fig. 4a). This is compared to a distribution of slopes of 83-yr AITG trends extracted from the corresponding preindustrial simulations (Fig. 4b). For each preindustrial simulation, overlapping 83-yr-trend slopes are calculated, starting at the first year and stepping the window forward in 1-yr increments. The estimated degrees of freedom of the preindustrial slope distribution are calculated conservatively by dividing, for each model, the length of the preindustrial simulation used (239 yr) by the length of the trend window (83 yr) and then summing this value across the various models.

The CMIP5 distribution is shifted in the positive direction, with the mean trend of  $0.109^{\circ}\text{C century}^{-1}$  (Fig. 4a,

dashed line) being significantly different at the 99% level (one-tailed  $t$  test) from the mean of the preindustrial distribution (Fig. 4a, dashed–dotted line). The CMIP5 historical-mean trend slope is only about half the magnitude of the observed AITG trend (Fig. 4a, solid line), but the observed trend magnitude is still well within the distribution of CMIP5 historical AITG trends. We note that the AITG trend distribution in the CMIP5 preindustrial simulations is comparable in width to the CMIP5 historical distribution, indicating that the range in the simulated AITG trend is largely due to internal variability. Thus, internal variations of the AITG offer a plausible explanation for the difference between the observed AITG trend and the CMIP ensemble-mean trend. However, we also cannot rule out the possibility that models may not be simulating the correct magnitude of the forced AITG trend. We discuss this topic further in section 6.

#### b. CMIP5 single-forcing runs

We examine single-forcing simulations to determine the cause(s) of the forced AITG trend in the CMIP5 historical runs. The available simulations are somewhat sparse (Table 1), and there is some ambiguity regarding what is incorporated into a particular single-forcing

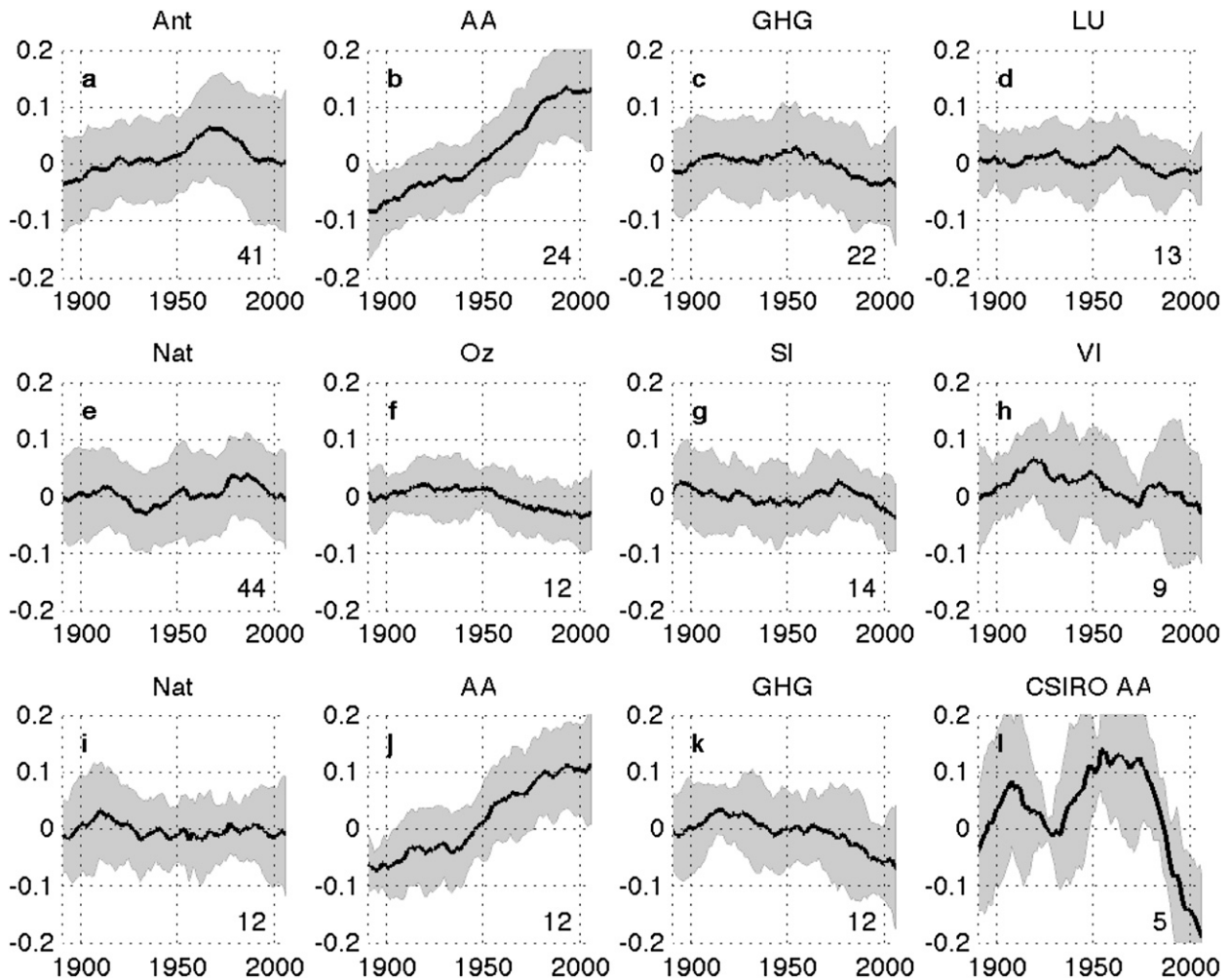


FIG. 5. The AITG as simulated by single-forcing runs listed in Table 1: (a)–(h) Ant, AA, GHG, LU, Nat, Oz, SI, and VI, respectively. The black line is the ensemble mean, and shading denotes one std dev above and below the mean. The number at the bottom right of each panel is the ensemble size. Note that, for (b), the CSIRO Mk3.6.0 anthropogenic aerosol members were excluded. (i)–(k) Nat, AA and GHG but limited to a consistent subset of models and ensemble members, comprising 1 CCSM4, 5 CanESM2, 3 GISS-E2-R, 1 IPSL-CM5A-LR, 1 NorESM1-M, and 1 GFDL-ESM2M member. (l) The 5 CSIRO Mk3.6.0 anthropogenic aerosol members.

category (so, e.g., anthropogenic aerosols may incorporate somewhat different microphysical treatment and aerosol mixes in different models). Thus, a fully controlled multimodel evaluation of the single-forcing simulations is not possible. On the other hand, we have many more single-forcing runs here than what was used in the Chang et al. (2011) CMIP3 study (they used seven members across three models per single-forcing set).

Some strong suggestions emerge from this analysis. Figures 5a–h show the AITG from all single-forcing simulations, grouped by forcing type. One result is immediately apparent: anthropogenic (Fig. 5a, derived from 41 members from 8 different models) rather than natural (Fig. 5e, derived from 47 members from 16 different models) forcing is responsible for both the

upward AITG trend prior to the late 1970s, as well as for the turnaround in the AITG trend after that period. The natural forcing-only simulations do not produce a discernible AITG trend.

The standout anthropogenic influence on the AITG trend is from anthropogenic aerosols, whose single-forcing simulations collectively show a pronounced positive trend throughout the twentieth century except at the end (Fig. 5b, derived from 24 members from 8 different models). Here, we excluded the CSIRO Mk3.6.0 members because their behaviors were significantly different from the others (see the end of this section for a discussion). Individually, all the individual anthropogenic aerosol members (again, excepting the CSIRO Mk3.6.0) exhibit upward trends. Interestingly, the time

evolution of the anthropogenic aerosol-only AITG resembles the time history of sulfate aerosol emissions over the North Atlantic sector (see Fig. 8 of Chang et al. 2011): there are two periods of emissions growth (from the middle to late 1800s until ~1920 and again from ~1940 through ~1980), with a hiatus from ~1920 to ~1940 and a reversal after the mid-1970s.

The conclusion of anthropogenic aerosol forcing driving the AITG trend can also be inferred separately from the other anthropogenic single-forcing runs. None of the other sources of anthropogenic forcing—greenhouse gases (Fig. 5c), land use (Fig. 5d), and ozone (Fig. 5f)—shows an upward trend, and in fact all hint at small downward trends. The implication is that the trend from the anthropogenic all-forcing runs originates from the only remaining sizable anthropogenic forcing group (i.e., anthropogenic aerosols). The small downward trend in the other anthropogenic forcings also likely explains why the upward trend in the all anthropogenic-forcing run is less than for the anthropogenic aerosol-forcing run.

The single-forcing simulations also suggest the origins of the late 1970s reversal in the AITG trend. There is also a flattening to the anthropogenic aerosol-only trend in the late twentieth century, consistent with the suggestion by Chang et al. (2011) that the reduction of atmospheric pollution helped cause a reversal in the AITG. However, greenhouse gas forcing also drove a fairly pronounced negative AITG trend after the 1970s (Fig. 5c), suggesting that it also contributed to the reversal in the AITG trend after the late 1970s. We think this is indeed the case; we discuss this further in section 4.

A drawback of our above analysis is that each single-forcing behavior is inferred from different sets of models in the composition. We address this by creating a composite of the single-forcing simulations that have the same model composition. Figures 5i–k show this comparison for the natural-, anthropogenic aerosol-, and greenhouse gas-forcing simulations respectively, combining 1 CCSM4 member, 5 CanESM2 members, 3 GISS-E2-R members, 1 IPSL-CM5A-LR member, 1 NorESM1-M member, and 1 GFDL-ESM2M member (for a total of 12 ensemble members). They confirm our assessment above that anthropogenic aerosol forcing produces a significant upward trend prior to the late twentieth century, whereas natural or greenhouse gas forcing does not.

Finally, we comment on the CSIRO Mk3.6.0 anthropogenic aerosol runs. They are distinctly different from the other models' anthropogenic aerosol runs, in that each member exhibits large multidecadal variability (Fig. 5l) very unlike the upward trend behavior of the anthropogenic aerosol runs of the other models (Fig. 5b).

The AMOC of the CSIRO model is quite sensitive to forcing: Collier et al. (2013) showed that the AMOC in the CSIRO Mk3.6.0 historical anthropogenic aerosol runs respond with a pronounced acceleration over the second half of the twentieth century, causing a warming of the North Atlantic. This would explain the downward trend in the CSIRO AITG simulations in the latter half of the twentieth century (Fig. 5l). Nevertheless, given that the other 8 models represented in the anthropogenic aerosol single-forcing runs individually show similar AITG upward trends, we regard the CSIRO Mk3.6.0 anthropogenic aerosol result as an outlier. Interestingly, the CSIRO Mk3.6.0 all-anthropogenic runs collectively show behavior similar to the multimodel-mean all-anthropogenic runs (not shown), so we can at least make that attribution from the CSIRO Mk3.6.0 runs.

### c. Comparison to CMIP3

The CMIP5 results are generally consistent with the CMIP3 results: namely,

- The most common AITG behavior, shared by most (but not all) models, is a trend whereby the south warms faster than the north over most of the twentieth century (Figs. 2, 3); in both cases, there is a reversal in the trend in the late 1970s;
- The mean historical AITG trends (pre-1980s) are significantly different from those simulated by the preindustrial simulation, indicating that a portion of the AITG trend is forced (Fig. 4).
- Anthropogenic aerosols are the main contributors to this AITG trend, though the lack of sulfate aerosol-only runs precludes us from making that specific attribution (Fig. 5).
- Anthropogenic aerosols also appear to partly cause the reversal of the AITG trend in the late 1970s; in addition [not found in Chang et al. (2011)], there also appears to be a role of greenhouse gases in causing this reversal.

The most significant difference is that 2 (of 25) CMIP5 models systematically simulate decreasing AITG trends (MPI-ESM-LR and MRI-CGCM3); this is clearly seen in the individual member AITG indices for those models (Fig. 2b, thin black lines), and also in the negative EOF1 loadings with these models (Fig. 3b). This is unlike the CMIP3, where no model (23 total) analyzed systematically produced decreasing AITG trends (Fig. 3d). As a consequence, the multimodel ensemble mean-forced trend is weaker in the CMIP5 ( $0.109^{\circ}\text{C century}^{-1}$ ) than in the CMIP3 ( $0.129^{\circ}\text{C century}^{-1}$ ). Excluding these two models from our analysis results in a multimodel-mean trend of  $0.139^{\circ}\text{C century}^{-1}$ , similar to CMIP3, and

the extreme negative contributions to the CMIP5 distribution (Fig. 4a, the  $-0.4^{\circ}$  and  $-0.3^{\circ}\text{C century}^{-1}$  entries) disappear. We do not know the reason why these two models exhibit negative AITG trends, but we will discuss this issue further in section 4.

The spread in the distribution of trend slopes—reflecting the uncertainty in the magnitude of the forced trend—has not been reduced in the CMIP5; if anything, it has slightly increased because of the two CMIP5 model outliers. We have not established the reasons for the negative AITG trend in the two CMIP5 models (though see the discussion in section 4), and we have no reason to exclude them from our analysis. Thus, while the conclusions from the CMIP5 remain the same as for the CMIP3, there is somewhat less confidence in the robustness of the conclusions because of the two CMIP5 model outliers.

#### 4. Northern and southern components of the AITG

We separately examine the behaviors of the northern and southern components of the AITG [northern tropical Atlantic (NTA) and southern tropical Atlantic (STA)] in order to further attribute causes of the AITG trend in section 3. If anthropogenic aerosols are indeed the primary driver of the trend before the late 1970s and the turnaround after that, then the influence should primarily be felt in the NTA because anthropogenic aerosols are largely located in the Northern Hemisphere. We also note that the NTA and STA SST variability has been previously shown to be uncorrelated over interannual–decadal time scales (Enfield et al. 1999; Houghton and Tourre 1992), indicating that each can evolve for different and possibly independent reasons.

Figure 6a (Fig. 6b) shows the spaghetti diagram for all CMIP5 ensemble simulations of the NTA (STA), and the dashed line gives the multimodel ensemble mean (excluding the outliers HadGEM2, MPI-ESM-LR, and MRI-CGCM3 as in Fig. 2b). For both NTA and STA indices there are three distinct periods of evolution, but with subtle differences that explain the multimodel-mean behavior of the AITG:

- From the late 1800s to the late 1940s: the small but distinct upward AITG trend is due to the slightly faster STA warming compared to the NTA.
- From the late 1940s to the late 1970s: the sharp upward rise in the AITG is driven primarily by a cooling NTA; the STA remains relatively flat.
- From the late 1970s onward: both the STA and NTA resume their warming trend, but this time with the NTA warming faster; this results in the AITG turnaround after that time.

All natural, anthropogenic aerosol, and greenhouse gas single-forcing simulations of the NTA and STA (shown in Figs. 6c,d, respectively) aid our interpretation of the CMIP5 multimodel-mean NTA and STA behavior (here, we use the same multimodel subset as in Figs. 5i–k to compute the ensemble means, so that the curves can be consistently compared). They reveal the following:

- From the late 1800s to the early 1950s: both greenhouse gas and natural forcings warm the NTA and STA and anthropogenic aerosols cool; however, the aerosol cooling is significantly stronger in the NTA than STA, accounting for the greater STA rise over the NTA during this period (and hence an upward AITG trend).
- From the late 1940s to the late 1970s: both greenhouse gases and anthropogenic aerosols continue their earlier trend, but the aerosol cooling accelerates in the NTA. Furthermore, natural forcings also start cooling both the NTA and STA. As a result, both the NTA and STA undergo cooling trends during this interval, with the NTA cooling being more pronounced.
- From the late 1970s onward: both the anthropogenic aerosol and natural influence on the NTA and STA flattens out; this allows the greenhouse gas influence to become strongly expressed in the NTA and STA. As a result, both the NTA and STA warm considerably during this period. Furthermore, greenhouse gases warm the NTA faster than the STA, resulting in the same for the NTA and STA in the all-forcing runs.

So, in summary, our separate NTA and STA analyses suggest that the upward AITG trend prior to the 1970s is due primarily to the fact that anthropogenic aerosols cooled the NTA more than the STA, in particular from the late 1940s to the late 1970s; after the late 1970s, the anthropogenic aerosol influence on the AITG leveled off. The temporal behaviors are consistent with our understanding of the anthropogenic aerosol influence on the historical climate, in particular with sulfate aerosols that dominate anthropogenic aerosol emissions. The  $\text{SO}_2$  emissions grew steadily from the 1800s but accelerated in pace since the 1950s until leveling off in the 1970s and falling thereafter (Lamarque et al. 2010). Also, the fact that the NTA cooled faster relative to the STA is consistent with a Northern Hemisphere anthropogenic  $\text{SO}_2$  source (Rotstajn and Lohmann 2002).

On the other hand, the reversal in the upward AITG trend after the late 1970s was a combination of the leveling off of the anthropogenic aerosol influence, combined with an increased influence of greenhouse gases that warmed the NTA faster than the STA. This result is parallel with a recent analysis by Friedman et al.

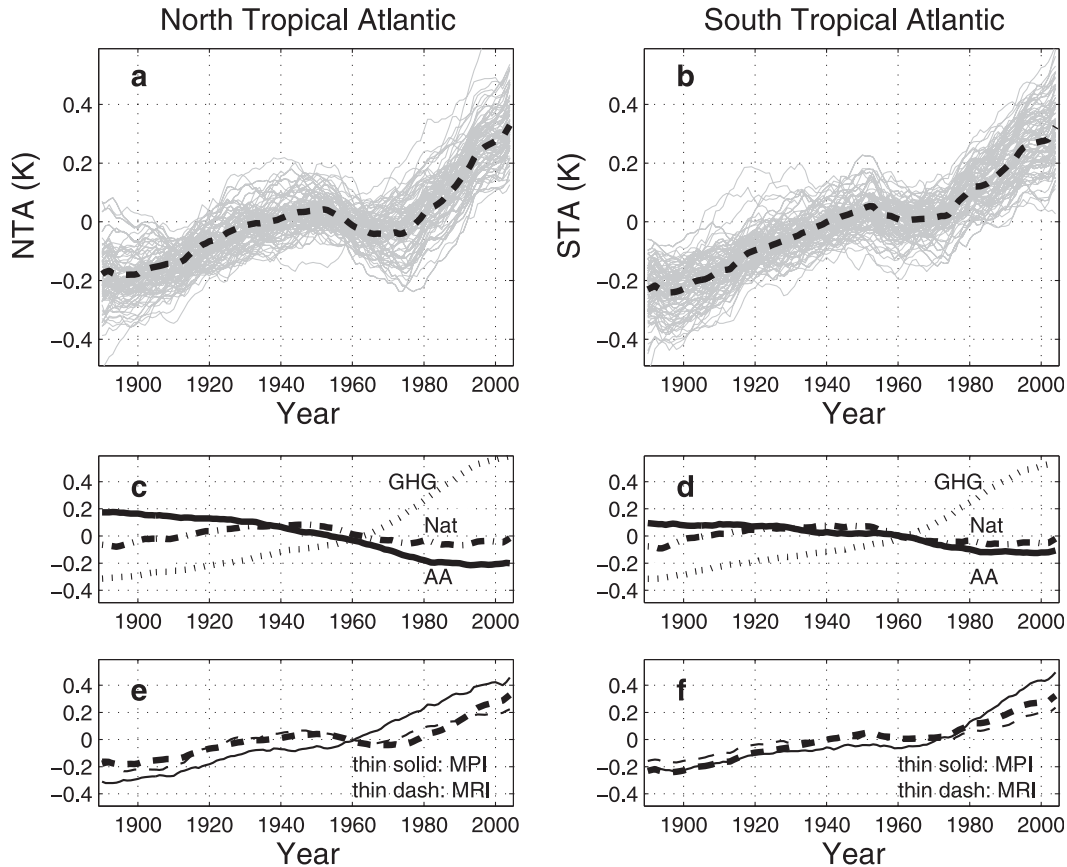


FIG. 6. CMIP5 simulations of (a) NTA and (b) STA. The light gray lines are the individual CMIP ensemble members, and the thick dashed line is the multimodel ensemble mean excluding the outlier HadGEM2, MPI-ESM-LR, and MRI-CGCM3 models. The figures indicate that the accelerated upward trend in the AITG beginning in the 1940s is due to a mild cooling of the NTA starting around that time; the STA stayed relatively flat. On the other hand, the reversal of the AITG trend post-1980 is due to the accelerated warming of the NTA at that time. (c) Single-forcing simulations of the NTA showing the ensemble-mean AA, GHG, and Nat. Here, we use the same multimodel subset as for Figs. 5i–k. (d) As in (c), but for the STA. (e) Comparing the NTA multimodel ensemble mean (thick dashed line) against the ensemble means of the MPI-ESM-LR (thin solid line) and MRI-CGCM3 (thin dashed line) simulations. (f) As in (e), but for the STA.

(2013) on the global interhemispheric surface temperature gradient (i.e., Northern Hemisphere versus Southern Hemisphere); they also found that the anthropogenic aerosol influence leveled off in the late 1970s, allowing the greenhouse gas forcing to dominate the change in the global interhemispheric gradient. Increased greenhouse gases warm the Northern Hemisphere (as a whole) faster than the Southern Hemisphere (Friedman et al. 2013), because of greater land area in the North as well as positive feedbacks (in particular from Arctic sea ice cover).

Finally, we briefly revisit the issue regarding the two models with negative AITG trends (MPI-ESM-LR and MRI-CGCM3; their NTA and STA simulations are shown in Figs. 6e,f, respectively). In both cases, their NTA and STA simulations are plausibly within the ensemble behavior; they both show two phases of warming in the early and late twentieth century, with a hiatus in

the middle of the century. However, it can also be seen that the total NTA variation over the twentieth century in these two models is larger than that for the STA, unlike the other models (and thus explaining the negative AITG trend). We conclude from this that the reasons for the different AITG behavior for MPI and MRI models is likely to be quite subtle, possibly having to do with how the NTA and STA separately respond to radiative forcing.

## 5. Multidecadal variations

Booth et al. (2012) showed that the HadGEM2-ES historical simulations generated AMO-like changes in North Atlantic SST, approximately matching the observed in both phase and amplitude: they quote that 75% of the detrended North Atlantic SST variation

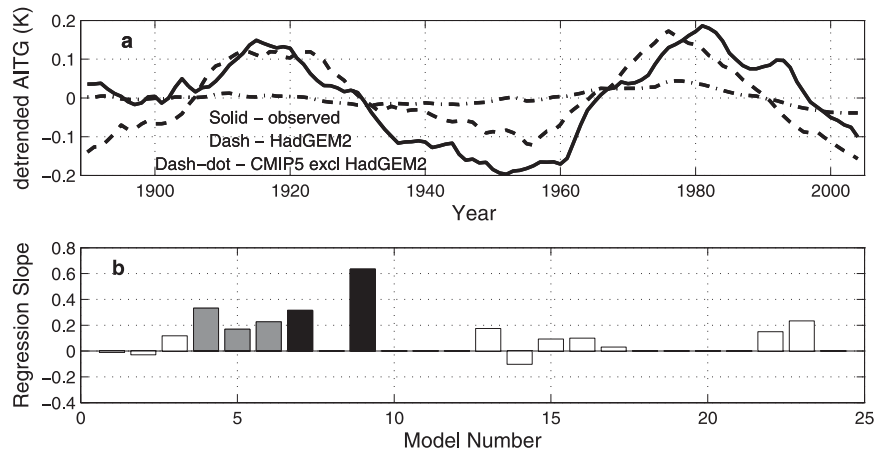


FIG. 7. (a) Multidecadal modulation in the AITG. The observed detrended AITG (where the AITG here is taken as the average of the three estimates shown in Fig. 1) is shown as the solid line. The dashed line is the average of the detrended AITG of the HadGEM2-CC and HadGEM2-ES historical simulations, and the dashed-dotted line is the average of all the other CMIP5 AITG indices excluding the HadGEM2-CC and HadGEM2-ES. (b) Regression slope of the observed detrended AITG [black line of (a)] with the simulated detrended AITG by each CMIP5 model with at least three historical members, from 1890 to 2004. For each model, we took the ensemble members available and averaged their detrended AITG; this was then regressed against the observed detrended AITG. The height of the bars represents the regression slope. Bars are shaded gray if the correlation between the observed and model mean AITG exceed  $r > 0.61$ , significant at the 90% level, and shaded black if the correlation exceeds  $r > 0.73$ , significant at the 95% level. The model corresponding to the model number can be looked up in Table 1; HadCM3 (model 7) and HadGEM-ES (model 9) are correlated at the 95% level, and CanESM2 (model 4), GISS-E2H (model 5), and GISS-E2-R (model 6) are correlated at the 90% level.

(smoothed over 10-yr intervals to highlight the multidecadal) is explained by the HadGEM2-ES historical simulations. They attributed this behavior to the radiative effects of imposed anthropogenic and volcanic aerosols on the SST, in particular indirect effects. Given a pronounced AMO influence in the observed AITG (Fig. 7a, solid line), we ask to what extent they occur in the CMIP5.

The 5 HadGEM simulations in our 85-member ensemble simulate an AMO-like signature in both phase and amplitude (Fig. 2a, thin black lines; the detrended HadGEM multimodel mean is shown in Fig. 7a, dashed line). However, the detrended AITG averaged across the remaining ensemble members (note that this mean includes the MPI-ESM-LR and MRI-CGCM3 models) show only a muted multidecadal modulation (Fig. 7a, dashed-dotted line). We further compared the multidecadal AITG simulations for each model against the observed, by computing the regression slope of each model's mean multidecadal behavior on the observed detrended AITG. Prior to regression, all AITG indices of a particular model were detrended and averaged (so we are examining the collective ability of that model to simulate the observed multidecadal variation). Only

models with at least three historical ensemble members were analyzed. The results (Fig. 7b) show that only 2 of 15 models with at least three historical members—HadCM3 and HadGEM2-ES—were correlated at the 95% level ( $r > 0.73$ , assuming  $N = 6$ , given that the AITG time series are smoothed with a 21-yr running mean). At the 90% level ( $r > 0.61$ ), three additional models—namely, CanESM2, GISS-E2H, and GISS-E2-R—exceeded this threshold. It is thus apparent that only a small subset of the CMIP5 models plausibly simulate AMO-like behavior in the AITG; moreover, the regression coefficients in Fig. 7b indicate that of them, only the HadGEM2-ES model simulated the AMO-like behavior with amplitudes comparable to the observed AMO.

## 6. Summary and discussion

We examined multidecadal and trend behavior of the Atlantic interhemispheric SST gradient in the CMIP5 historical simulations, following previous CMIP3 analyses (Chang et al. 2011). Our results confirm the major conclusions of the previous study that at least a portion of the historical trend in the AITG was likely forced and by

anthropogenic aerosols. Given previous work that established the causal link between the Atlantic ITCZ and the AITG, we thus conclude that human activity likely contributed to the southward trend of the Atlantic ITCZ over the twentieth century. However, the CMIP5 ensemble-mean trend magnitude is only about half the observed AITG trend magnitude. Our analysis suggests that internal variations offer a plausible explanation to account for this difference. However, it is also possible that the simulated magnitude in the forced AITG trend may be underestimated. We discuss these further toward the end of this section.

The CMIP5 single-forcing simulation results appear to unambiguously reveal the influence of anthropogenic aerosols in forcing the model trend; no other forcing exhibits the increasing AITG trend with comparable magnitude of the slope and consistency across ensemble members. Similar to CMIP3, CMIP5 also produces a reversal in the AITG trend around 1980, further evidence that this reversal is forced. Our attribution analysis suggests that this reversal is due to anthropogenic forcing, partly from the leveling off of the anthropogenic aerosol influence but also because of the increased influence of greenhouse gases, in the late twentieth century. We have far greater confidence in the attribution results of this study compared to Chang et al. (2011) because of the far greater number of single-forcing runs used here. However, a definitive attribution requires that we are able to also tie the intermodel differences in the AITG simulation to intermodel differences in the applied historical forcing, something that we have not done in this analysis.

With regards to forced multidecadal variations in the AITG, our conclusion is that the HadGEM2 models are the only ones that express AMO-like multidecadal variations with the correct phase and amplitude. A few others (CanESM2, GISS-E2H, GISS-E2-R, and HadCM3) do simulate AITG multidecadal behavior that is significantly correlated to the observed AMO-like behavior. It suggests that there may be sufficient information in the applied CMIP5 historical climate forcings to drive AMO-like behavior in the AITG, even if the amplitude of variation does not approach observed levels.

A stronger conclusion regarding the anthropogenic influence on the historical AITG and the role of aerosols remain elusive. Both CMIP3 and CMIP5 significantly underestimate the magnitude of the AITG trend compared to the observed, and there is also substantial spread in the simulated trends. The latter is likely due to internal variations of the climate system, given that the preindustrial simulations also produce a similar spread in simulated AITG trends. Variations in the AMOC strength are the most likely source of unforced AITG

trends, given that they have long time scales and significantly affect the AITG (e.g., Knight et al. 2005).

However, it is also possible that uncertainty in representation of aerosol forcing in climate models may also contribute to the difference between the observed and ensemble-mean AITG trend, as well to the spread in the simulated AITG trends. Since the CMIP3, there has been a concerted effort by various modeling groups to improve the representation of historical aerosol forcing, both direct and indirect, in coupled models. In particular, based on results of our previous analysis with the CMIP3 (Chang et al. 2011), we anticipated that the near-universal inclusion of indirect effects in the CMIP5-class models would result in a larger simulated AITG trend, more closely matching the observed trend. However (and to our surprise), neither the CMIP5 AITG trends magnitude nor spread appreciably changed from the CMIP3.

*Acknowledgments.* We acknowledge the World Climate Research Programme's Working Group on Coupled Modelling, which is responsible for CMIP, and we thank the climate modeling groups (listed in Table 1 of this paper) for producing and making available their model output. For CMIP the U.S. Department of Energy's Program for Climate Model Diagnosis and Intercomparison provides coordinating support and led development of software infrastructure in partnership with the Global Organization for Earth System Science Portals. This research was supported by NSF AGS-1126351, as part of a diagnostic analysis effort proposed by U.S. CLIVAR, and the Department of Energy, Office of Science (BER) (DE-FG02-08ER64588). JCHC also acknowledges support from the Consortium for Climate Change Study of Taiwan during his sabbatical in Academia Sinica January–June 2012. MFW was supported by the Regional and Global Climate Modeling Program and by the Earth System Modeling Program of the Office of Biological and Environmental Research in the Department of Energy Office of Science (DE-AC02-05CH11231). We thank Andrew Friedman for assistance with the obtaining and processing CMIP5 output; Mike Wallace, Leon Rotstayn, Ka-Kit Tung, and three anonymous reviewers for their comments on the original submission; and Wei Cheng and Abigail Swann for useful discussions.

## REFERENCES

- Barnett, T. P., 1977: Principal time and space scales of Pacific trade wind fields. *J. Atmos. Sci.*, **34**, 221–236.
- Booth, B. B. B., N. J. Dunstone, P. R. Halloran, T. Andrews, and N. Bellouin, 2012: Aerosols implicated as a prime driver of twentieth-century North Atlantic climate variability. *Nature*, **484**, 228–232.

- Chang, C. Y., J. C. H. Chiang, M. F. Wehner, A. R. Friedman, and R. Ruedy, 2011: Sulfate aerosol control of tropical Atlantic climate over the twentieth century. *J. Climate*, **24**, 2540–2555.
- Chang, P., R. Saravanan, L. Ji, and G. C. Hegerl, 2000: The effect of local sea surface temperatures on the atmospheric circulation over the tropical Atlantic sector. *J. Climate*, **13**, 2195–2216.
- Chiang, J. C. H., and A. R. Friedman, 2012: Extratropical cooling, interhemispheric thermal gradients, and tropical climate change. *Annu. Rev. Earth Planet. Sci.*, **40**, 383–412.
- , Y. Kushnir, and A. Giannini, 2002: Deconstructing Atlantic intertropical convergence zone variability: Influence of the local cross-equatorial sea surface temperature gradient and remote forcing from the eastern equatorial Pacific. *J. Geophys. Res.*, **107**, doi:10.1029/2000JD000307.
- Collier, M. A., L. D. Rotstayn, K.-Y. Kim, A. C. Hirst, and S. J. Jeffrey, 2013: Ocean circulation response to anthropogenic-aerosol and greenhouse-gas forcing in the CSIRO-Mk3.6 coupled climate model. *Aust. Meteor. Oceanogr. J.*, **63**, 27–39.
- Cox, P. M., and Coauthors, 2008: Increasing risk of Amazonian drought due to decreasing aerosol pollution. *Nature*, **453**, 212–217.
- Enfield, D. B., A. M. Mestas-Nunez, D. A. Mayer, and L. Cid-Serrano, 1999: How ubiquitous is the dipole relationship in tropical Atlantic sea surface temperatures? *J. Geophys. Res.*, **104** (C4), 7841–7848.
- Friedman, A. R., Y.-T. Hwang, J. C. H. Chiang, and D. M. W. Frierson, 2013: Interhemispheric temperature asymmetry over the twentieth century and in future projections. *J. Climate*, **26**, 5419–5433.
- Hastenrath, S., and L. Heller, 1977: Dynamics of climatic hazards in northeast Brazil. *Quart. J. Roy. Meteor. Soc.*, **103**, 77–92.
- Houghton, R. W., and Y. M. Tourre, 1992: Characteristic low-frequency sea surface temperature fluctuations in the tropical Atlantic. *J. Climate*, **5**, 765–771.
- Kang, S. M., D. M. W. Frierson, and I. M. Held, 2009: The tropical response to extratropical thermal forcing in an idealized GCM: The importance of radiative feedbacks and convective parameterization. *J. Atmos. Sci.*, **66**, 2812–2827.
- Kaplan, A., M. A. Cane, Y. Kushnir, A. C. Clement, M. B. Blumenthal, and B. Rajagopalan, 1998: Analyses of global sea surface temperature 1856–1991. *J. Geophys. Res.*, **103** (C9), 18 567–18 589.
- Knight, J. R., R. J. Allan, C. K. Folland, M. Vellinga, and M. E. Mann, 2005: A signature of persistent natural thermohaline circulation cycles in observed climate. *Geophys. Res. Lett.*, **32**, L20708, doi:10.1029/2005GL024233.
- Lamarque, J.-F., and Coauthors, 2010: Historical (1850–2000) gridded anthropogenic and biomass burning emissions of reactive gases and aerosols: Methodology and application. *Atmos. Chem. Phys.*, **10**, 7017–7039.
- Meehl, G. A., C. Covey, T. Delworth, M. Latif, B. McAvaney, J. F. B. Mitchell, R. J. Stouffer, and K. E. Taylor, 2007: THE WCRP CMIP3 multimodel dataset: A new era in climate change research. *Bull. Amer. Meteor. Soc.*, **88**, 1383–1394.
- Moura, A. D., and J. Shukla, 1981: On the dynamics of droughts in northeast Brazil: Observations, theory and numerical experiments with a general circulation model. *J. Atmos. Sci.*, **38**, 2653–2675.
- Rayner, N. A., D. E. Parker, E. B. Horton, C. K. Folland, L. V. Alexander, D. P. Rowell, E. C. Kent, and A. Kaplan, 2003: Global analyses of sea surface temperature, sea ice, and night marine air temperature since the late nineteenth century. *J. Geophys. Res.*, **108**, 4407, doi:10.1029/2002JD002670.
- Rotstayn, L. D., and U. Lohmann, 2002: Tropical rainfall trends and the indirect aerosol effect. *J. Climate*, **15**, 2103–2116.
- Smith, T. M., R. W. Reynolds, T. C. Peterson, and J. Lawrimore, 2008: Improvements to NOAA's historical merged land-ocean surface temperature analysis (1880–2006). *J. Climate*, **21**, 2283–2296.
- Taylor, K. E., R. J. Stouffer, and G. A. Meehl, 2012: An overview of CMIP5 and the experiment design. *Bull. Amer. Meteor. Soc.*, **93**, 485–498.
- Ting, M. F., Y. Kushnir, R. Seager, and C. H. Li, 2009: Forced and internal twentieth-century SST trends in the North Atlantic. *J. Climate*, **22**, 1469–1481.
- Williams, K. D., A. Jones, D. L. Roberts, C. A. Senior, and M. J. Woodage, 2001: The response of the climate system to the indirect effects of anthropogenic sulfate aerosol. *Climate Dyn.*, **17**, 845–856.